J. Fluid Mech. (2013), *vol.* 719, *pp.* 183–202.
doi:10.1017/jfm.2012.639

Sensitivity analysis of a time-delayed thermo-acoustic system via an adjoint-based approach

Luca Magri† and Matthew P. Juniper

Department of Engineering, University of Cambridge, Trumpington Street, Cambridge CB2 1PZ, UK

(Received 25 July 2012; revised 1 November 2012; accepted 17 December 2012)

We apply adjoint-based sensitivity analysis to a time-delayed thermo-acoustic system: a Rijke tube containing a hot wire. We calculate how the growth rate and frequency of small oscillations about a base state are affected either by a generic passive control element in the system (the structural sensitivity analysis) or by a generic change to its base state (the base-state sensitivity analysis). We illustrate the structural sensitivity by calculating the effect of a second hot wire with a small heat-release parameter. In a single calculation, this shows how the second hot wire changes the growth rate and frequency of the small oscillations, as a function of its position in the tube. We then examine the components of the structural sensitivity in order to determine the passive control mechanism that has the strongest influence on the growth rate. We find that a force applied to the acoustic momentum equation in the opposite direction to the instantaneous velocity is the most stabilizing feedback mechanism. We also find that its effect is maximized when it is placed at the downstream end of the tube. This feedback mechanism could be supplied, for example, by an adiabatic mesh. We illustrate the base-state sensitivity by calculating the effects of small variations in the damping factor, the heat-release time-delay coefficient, the heat-release parameter, and the hot-wire location. The successful application of sensitivity analysis to thermo-acoustics opens up new possibilities for the passive control of thermo-acoustic oscillations by providing gradient information that can be combined with constrained optimization algorithms in order to reduce linear growth rates.

Key words: acoustics, flow control, instability control

1. Introduction

In a thermo-acoustic system, heat-release oscillations couple with acoustic-pressure oscillations. If the heat release is sufficiently in phase with the pressure, these oscillations grow, sometimes with catastrophic consequences. Using adjoint sensitivity analysis, we identify the most influential components of a thermo-acoustic system and quantify their influence on the frequency and growth rate of oscillations. This technique shows how a thermo-acoustic system should be changed in order to extend its linearly stable region.

† Email address for correspondence: lm547@cam.ac.uk

Adjoint sensitivity analysis of incompressible flows was proposed by Hill (1992) and developed further by Giannetti & Luchini (2007) in order to reveal the region of the flow that causes a von Kármán vortex street behind a cylinder. They used adjoint methods to calculate the effect that a small control cylinder has on the growth rate of oscillations, as a function of the control cylinder's position downstream of the main cylinder. This control cylinder induces a force in the opposite direction to the velocity field. Giannetti & Luchini (2007) and Giannetti, Camarri & Luchini (2010) considered this feedback only on the perturbed fields but Marquet, Sipp & Jacquin (2008) extended this analysis to consider the cylinder's effect on the base flow as well. Sipp *et al.* (2010) provide a comprehensive review of sensitivity analysis for incompressible fluids and Chandler *et al.* (2012) extend this analysis to low-Mach-number flows in order to model variable-density fluids and flames.

The aim of this paper is to extend adjoint sensitivity analysis to a thermo-acoustic system, which has not been attempted before. We investigate the thermo-acoustic system described by Balasubramanian & Sujith (2008*a*) and Juniper (2011). This is an open-ended tube, through which air passes, and which contains a hot wire at a given axial location. One-dimensional acoustic standing waves in the tube modulate the air velocity at the wire, which in turn modulates the heat transfer from the wire to the air, which is modelled with a modified form of King's law (Heckl 1990; Matveev 2003). This heat transfer occurs at the wire's location but is not instantaneous. The time taken for the heat to diffuse to the bulk fluid is modelled as a time delay between the velocity fluctuations and the heat-release fluctuations.

The analysis consists of three main steps. First, we study the system as an eigenvalue problem in the complex frequency domain. Secondly, we derive two sets of adjoint equations from the linearized governing equations. Thirdly, we use the adjoint equations to perform both a structural sensitivity analysis and a base-state sensitivity analysis. The structural sensitivity analysis quantifies the effect that feedback mechanisms have on the frequency and growth rate of oscillations. This analysis relies on studying the effect of a perturbation to the governing equations, which is known as a structural perturbation. There are several components of the feedback and, in this paper, we calculate all of them. We then illustrate the structural sensitivity by considering the effect of feedback from a second hot wire. The base-state sensitivity analysis quantifies the effect of a change in the constant coefficients of the governing equations. It does not involve a feedback mechanism. The base state in this thermo-acoustic model is represented by four parameters: the damping factor, ζ; the heat-release time-delay coefficient, τ; the heat-release parameter, β, and the hot-wire location, x_h. This shows us how to change these parameters in order to stabilize the system most. In addition, we can also calculate the location of the first hot wire that makes the system most sensitive to base-state modifications. In the final section we apply this analysis to the passive control of an unstable nonlinear system.

2. Thermo-acoustic model

The thermo-acoustic system examined in this paper is a horizontal Rijke tube containing a hot wire. It is governed by the following nonlinear time-delayed equations:

$$\frac{\partial u}{\partial t} + \frac{\partial p}{\partial x} = 0, \tag{2.1}$$

$$\frac{\partial p}{\partial t} + \frac{\partial u}{\partial x} + \zeta p - \dot{q} = 0, \tag{2.2}$$

$$\dot{q} = \frac{2}{\sqrt{3}}\beta \left(\left| \frac{1}{3} + u(t-\tau) \right|^{1/2} - \left(\frac{1}{3} \right)^{1/2} \right) \delta(x - x_h), \tag{2.3}$$

where u, p and $\dot{q}$ are the non-dimensional velocity, pressure, and heat-release rate, respectively. The hot wire is placed at $x = x_h$, which is modelled by the Dirac delta (generalized) function $\delta(x - x_h)$. The system has four control parameters: ζ, which is the damping; β, which encapsulates all relevant information about the hot wire, base velocity, and ambient conditions; τ, which is the time delay; and x_h, which is the position of the hot wire. The values of β, τ and x_h are given in the figure captions along with the damping constants c_1 and c_2. In § 3 we will explain how ζ is related to c_1 and c_2. Equations (2.1)–(2.2) are derived from the Navier–Stokes and energy equations by assuming first-order acoustics, as explained in Culick (1971). The heat-release rate in (2.3) is modelled with a modified form of King's law (Heckl 1990; Matveev 2003). Note that throughout this paper we define the heat-release parameter β to be $\sqrt{3}/2$ times the heat-release parameter β defined in Juniper (2011). The heat-release term (2.3) is linearized around a fixed point of the system, where $|u| \ll 1$. In addition, (2.3) is also linearized in time, assuming that the time-delay coefficient is sufficiently small compared with the period of the highest Galerkin mode (§ 3):

$$\dot{q} = \beta \left(u - \tau \frac{\partial u}{\partial t} \right) \delta(x - x_h). \tag{2.4}$$

By substituting (2.1) into (2.4), we obtain an equivalent expression for the linearized heat-release law:

$$\dot{q} = \beta \left(u + \tau \frac{\partial p}{\partial x} \right) \delta(x - x_h). \tag{2.5}$$

It is important to anticipate that, although (2.4) is physically equivalent to (2.5), the systems of the linearized governing equations (2.1), (2.2), (2.4) and (2.1), (2.2), (2.5) will produce two different sets of adjoint equations (§ 4).

3. Numerical discretization

The partial differential equations (2.1), (2.2), (2.4), which govern the thermo-acoustic system, are discretized into a set of ordinary differential equations by choosing an orthogonal basis that matches the boundary conditions. This procedure is also known as the Galerkin method. The variables are expressed as:

$$u(x,t) = \sum_{j=1}^{N} \eta_j(t) \cos(j\pi x), \quad p(x,t) = -\sum_{j=1}^{N} \left(\frac{\dot{\eta}_j(t)}{j\pi} \right) \sin(j\pi x). \tag{3.1}$$

The state of the system is given by the amplitudes of the Galerkin modes that represent velocity, η_j, and those that represent pressure, $\dot{\eta}_j/j\pi$. The state vector of the discretized system is the column vector $\boldsymbol{\chi} \equiv (\boldsymbol{u}, \boldsymbol{p})^{\mathrm{T}}$, where $\boldsymbol{u} \equiv (\eta_1, \ldots, \eta_N)^{\mathrm{T}}$ and $\boldsymbol{p} \equiv (\dot{\eta}_1/\pi, \ldots, \dot{\eta}_N/N\pi)^{\mathrm{T}}$. The discretized problem can be represented in matrix notation:

$$\frac{\mathrm{d}\boldsymbol{\chi}}{\mathrm{d}t} = \boldsymbol{\Gamma}\boldsymbol{\chi}, \tag{3.2}$$

where $\boldsymbol{\Gamma}$ is the $2N \times 2N$ direct matrix and $\boldsymbol{\chi}$ is the $2N \times 1$ state vector. The basis functions, $\cos(j\pi x)$ and $\sin(j\pi x)$, are the eigenfunctions of the undamped acoustic

system without the heater. The direct matrix $\boldsymbol{\Gamma}$ is given in appendix A in (A 2). Note that, when the system has N Galerkin modes, it has $2N$ degrees of freedom.

The linearized equations in § 2 are valid for small $|u_h|$ and $\tau \ll T_j$, where $T_j = 2/j$ is the period of the jth Galerkin mode, as explained in Juniper (2011). The results are presented here for a system with 10 Galerkin modes (as for system C in Juniper 2011). We checked modal convergence by considering more Galerkin modes and found that 10 modes provide an accurate representation of the system, as discussed in § 7.3.

At the ends of the tube, p and $\partial u/\partial x$ are both set to zero, which means that the system cannot dissipate acoustic energy by doing work on the surroundings. Dissipation and end losses are modelled by the damping parameter for each mode $\zeta_j = c_1 j^2 + c_2\sqrt{j}$, where c_1 and c_2 are constants. Oscillations of higher Galerkin modes decay very rapidly if no mechanism drives them. This damping model was used in Balasubramanian & Sujith (2008*b*) and was based on correlations developed by Matveev (2003) from models in Landau & Lifshitz (1959).

4. Adjoint operator

In this section the *adjoint operator* is defined. This definition is an extension over the time domain of the definition given by Dennery & Krzywicki (1996). Let L be a partial differential operator of order M acting on the function $q(x_1, x_2, \ldots, x_K, t)$, where K is the space dimension, such that $\mathrm{L}q(x_1, x_2, \ldots, x_K, t) = 0$. We refer to the operator L as the *direct operator* and the function q as the *direct variable*. The adjoint operator L^+ and adjoint variable q^+ are defined via the *generalized Green's identity*:

$$\int_0^{\mathrm{T}} \int_V \bar{q}^+ \mathrm{L}q - q\left(\overline{\mathrm{L}^+ q^+}\right) \,\mathrm{d}V\,\mathrm{d}t = \int_0^{\mathrm{T}} \int_S \sum_{i=1}^{K} \left[\frac{\partial}{\partial x_i} Q_i\left(q, \bar{q}^+\right)\right] n_i \,\mathrm{d}S\,\mathrm{d}t + \cdots$$
$$\cdots + \int_V Q_i(q, \bar{q}^+)\big|_0^{\mathrm{T}} \,\mathrm{d}V, \tag{4.1}$$

where $i = 1, 2, \ldots, K$ and $Q_i(q, \bar{q}^+)$ are functions which depend bilinearly on q, $\bar{q}^+$ and their first $M - 1$ derivatives. The complex-conjugate operation is labelled by an overline. The domain V is enclosed by the surface S, for which n_i are the projections on the coordinate axis of the unit vector in the direction of the outward normal to the surface dS. The time interval is T. The adjoint boundary conditions and initial conditions on the function q^+ are defined as those that make the right-hand side of (4.1) vanish identically on S, $t = 0$ and $t = T$.

The adjoint equations can either be derived from the continuous direct equations and then discretized (CA, discretization of the continuous adjoint) or be derived directly from the discretized direct equations (DA, discrete adjoint). For the CA method (§§ 6.1 and 6.2), the adjoint equations are derived by integrating the continuous direct equations by parts and then applying Green's identity (4.1). They are then discretized with the Galerkin method (3.1). The appendices of Juniper (2011) show the intermediate steps. Two different sets of adjoint equations are derived here, shown in table 1. The first set, CA_1, is obtained from (2.1), (2.2), (2.4) and produces the discretized adjoint matrix (A 3). The second set, CA_2, is obtained from (2.1), (2.2), (2.5) and produces the discretized adjoint matrix (A 4). The difference arises merely because the governing equations are arranged differently. It has no physical significance. For the DA method (§ 6.3) the adjoint is simply the negative Hermitian of the direct matrix: $\boldsymbol{\Phi} = -\boldsymbol{\Gamma}^H$.

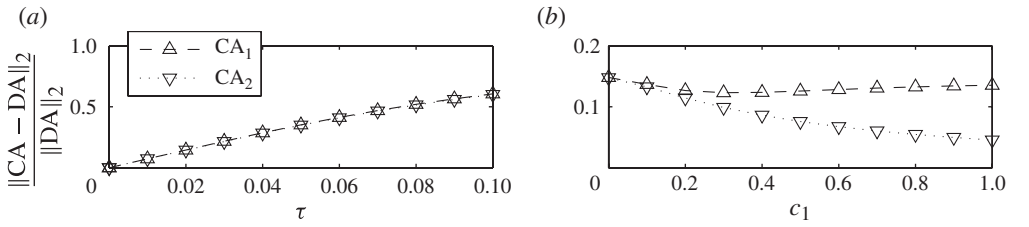

FIGURE 1. The discrepancy between the DA and the CA discretizations, for the two different formulations of the CA equations, CA_1 and CA_2. In both figures, $N = 10$, $x_h = 0.25$, and $\beta = 0.5$. (*a*) $c_1 = 0.01$, $c_2 = 0.004$ and (*b*) $c_2 = 0$, $\tau = 0.01$.

CA_1	CA_2
$\dfrac{\partial u^+}{\partial t} + \dfrac{\partial p^+}{\partial x} + \beta\left(p^+ + \tau\dfrac{\partial p^+}{\partial t}\right)\delta(x - x_h) = 0$	$\dfrac{\partial u^+}{\partial t} + \dfrac{\partial p^+}{\partial x} + \beta p^+\delta(x - x_h) = 0$
$\dfrac{\partial u^+}{\partial x} + \dfrac{\partial p^+}{\partial t} - \zeta p = 0$	$\dfrac{\partial u^+}{\partial x} + \dfrac{\partial p^+}{\partial t} - \zeta p - \beta\tau\dfrac{\partial[p^+\delta(x - x_h)]}{\partial x} = 0$

TABLE 1. The two different sets of continuous adjoint equations.

The DA method has the same truncation errors as the discretized direct system, while methods CA_1 and CA_2 have different truncation errors. The effect of these truncation errors is quantified in figure 1, which compares the discrepancy between CA_1 and DA with the discrepancy between CA_2 and DA. Method CA_1 has generally a greater discrepancy than CA_2, as shown in figure 1. This discrepancy is a function of the time delay, τ, and the damping coefficients, c_1 and c_2. Regardless of the value of the damping, the discrepancy is zero when $\tau = 0$. This can be inferred by examining the mathematical structure of the matrices given in (A 2), (A 3) and (A 4). If $\tau = 0$ then $\boldsymbol{\Phi} = -\boldsymbol{\Gamma}^H$ regardless of the formulation used.

These adjoint equations govern the evolution of the adjoint variables, which can be regarded as Lagrange multipliers from a constrained optimization perspective (Belegundu & Arora 1985). Therefore, u^+ is the Lagrange multiplier of the acoustic momentum equation (2.1). Physically, it reveals the spatial distribution of the system's sensitivity to a force. Likewise, p^+ is the Lagrange multiplier of the pressure equation (2.2) and (2.4) as well as (2.2) and (2.5). Physically, it reveals the spatial distribution of the system's sensitivity to heat injection.

5. Modal analysis: the eigenvalue problem

So far we have considered the thermo-acoustic system in the (x, t) domain. In modal analysis, we consider it in the (x, σ) domain using the transformations

$$u(x, t) = \hat{u}(x, \sigma)\mathrm{e}^{\sigma t}, \quad u^+(x, t) = \hat{u}^+(x, \sigma)\mathrm{e}^{-\bar{\sigma} t}, \tag{5.1}$$

$$p(x, t) = \hat{p}(x, \sigma)\mathrm{e}^{\sigma t}, \quad p^+(x, t) = \hat{p}^+(x, \sigma)\mathrm{e}^{-\bar{\sigma} t}, \tag{5.2}$$

where the symbol $\hat{}$ denotes an eigenfunction. The behaviour of the system in the long time limit is dominated by the eigenfunction whose eigenvalue has the highest growth rate. The complex-conjugate adjoint eigenfunctions of velocity and pressure are

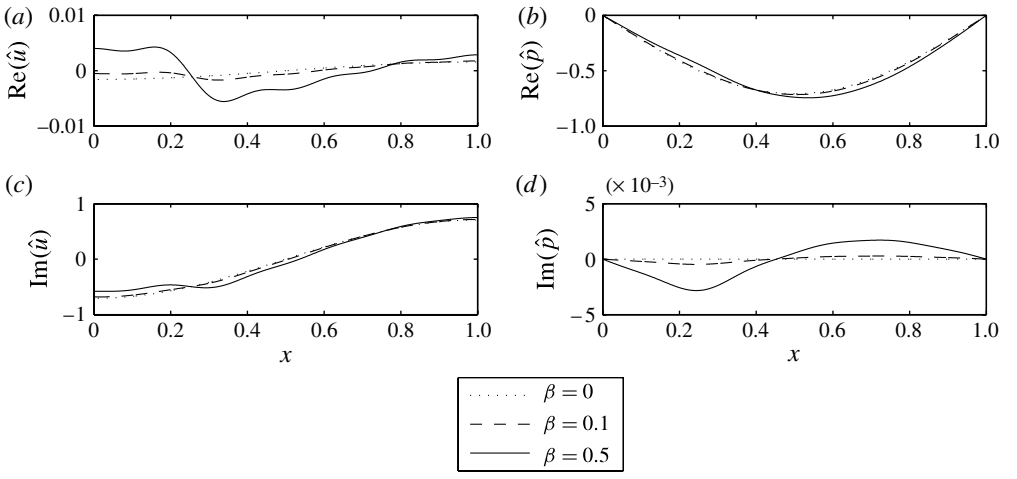

FIGURE 2. The direct eigenfunctions as a function of the heat-release parameter, β, for $N = 10$, $x_h = 0.25$, $\tau = 0.01$, $c_1 = 0.01$ and $c_2 = 0.004$. The relevant eigenvalues are: $\sigma = -0.0070 + 3.1416\mathrm{i}$, for $\beta = 0$; $\sigma = -0.0056 + 3.1848\mathrm{i}$, for $\beta = 0.1$; $\sigma = +0.00023 + 3.3570\mathrm{i}$, for $\beta = 0.5$. Note that (a) and (d) have very small vertical scales.

labelled $\hat{\tilde{u}}$ and $\hat{\tilde{p}}$, respectively. With the definition of the Green's identity (4.1), the adjoint eigenvalues, $-\bar{\sigma}$, are the negatives of the complex conjugates of the direct eigenvalues, σ. This satisfies the bi-orthogonality condition between the direct and adjoint eigenfunctions (Salwen & Grosch 1981). The system is studied in the complex frequency domain by substituting the relations (5.1) and (5.2) into the direct (2.1), (2.2), (2.4) and into the adjoint equations given in table 1.

Figure 2 shows the direct eigenfunctions and figure 3 the DA adjoint eigenfunctions as β increases from 0 to 0.5. When $\beta = 0$, the eigenfunctions are the natural acoustic modes of the duct but, as β increases, the eigenfunctions become distorted by the heat release at the wire. This has important consequences for the structural sensitivity, as will be shown in § 7.

Figure 4 shows the direct and adjoint eigenfunctions, found using the DA, CA_1, and CA_2 methods, at $\beta = 0.5$. This is the value of β used for the sensitivity analyses. The discrepancies in $\mathrm{Im}(u^+)$ and $\mathrm{Re}(p^+)$ cause the differences in sensitivities seen in §§ 7.1 and 7.4.

6. Calculation of the structural and base-state sensitivities

6.1. *Structural sensitivity via the* CA *method*

The thermo-acoustic system described in § 2 has been linearized about a base state. Following Giannetti & Luchini (2007), we perturb the linearized operator, L, by adding to it some general function of the perturbation state variables, $\hat{u}$ and $\hat{p}$. In this section, we assume that this feedback does not affect the base state. We also assume that the structural perturbation is small enough for the new thermo-acoustic configuration to be

$$\sigma_{new} = \sigma + \delta\sigma, \quad \hat{p}_{new} = \hat{p} + \delta\hat{p}, \quad \hat{u}_{new} = \hat{u} + \delta\hat{u}, \tag{6.1}$$

where $\delta\sigma = \epsilon\sigma$, $\delta\hat{p} = \epsilon\hat{p}$, $\delta\hat{u} = \epsilon\hat{u}$ with $|\epsilon| \ll 1$, and where terms of order ϵ^2 are sufficiently small to be neglected.

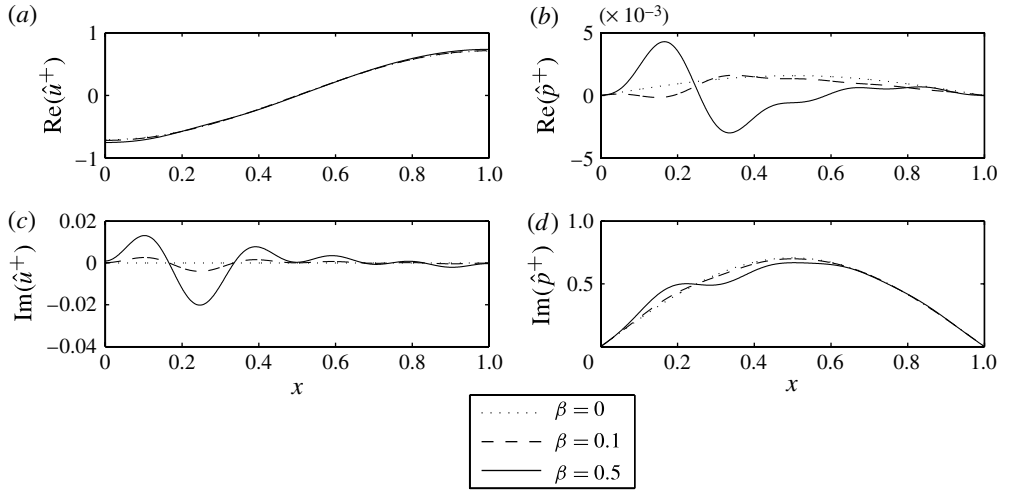

FIGURE 3. The adjoint eigenfunctions as a function of the heat-release parameter, β, for $N = 10$, $x_h = 0.25$, $\tau = 0.01$, $c_1 = 0.01$ and $c_2 = 0.004$. Note that (*b*) and (*c*) have very small vertical scales.

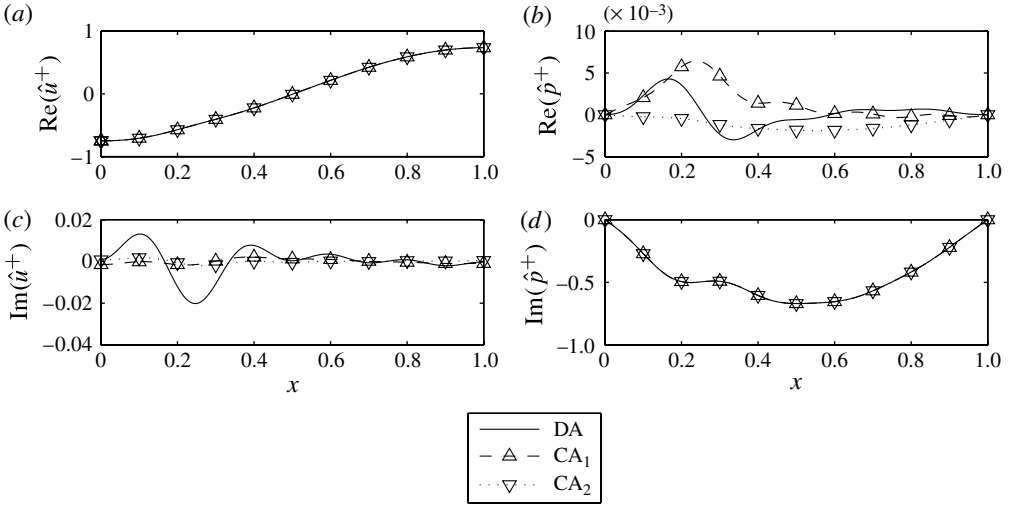

FIGURE 4. The adjoint eigenfunctions found using the DA, CA_1, and CA_2 methods. The parameters are $N = 10$, $x_h = 0.25$, $\tau = 0.01$, $\beta = 0.5$, $c_1 = 0.01$ and $c_2 = 0.004$. Note that (*b*) and (*c*) have very small vertical scales.

The direct eigenfunctions can be arranged as a column vector $[\hat{u} \quad \hat{p}]^{\mathrm{T}}$. In general, a structural perturbation to the thermo-acoustic operator can be represented by a 2×2 tensor, $\delta\boldsymbol{H}$, which acts on $[\hat{u} \quad \hat{p}]^{\mathrm{T}}$. Each component δH_{ij} of this structural perturbation tensor quantifies the effect of a feedback mechanism between the jth eigenfunction and the ith direct governing equation.

We obtain the eigenvalue drift, $\delta\sigma$, caused by the structural perturbation, $\delta\boldsymbol{H}$, by applying the Green's identity (4.1) to the perturbed direct and adjoint equations, in

Method	CA_1	CA_2
$\delta\sigma =$	$\dfrac{\int_L [\hat{\tilde{u}}^+ \quad \hat{\tilde{p}}^+]\delta\boldsymbol{H}[\hat{u} \quad \hat{p}]^{\mathrm{T}}\,\mathrm{d}x}{\int_L (\hat{u}\hat{\tilde{u}}^+ + \hat{p}\hat{\tilde{p}}^+)\,\mathrm{d}x + \beta\tau\hat{u}_h\hat{\tilde{p}}_h^+}$	$\dfrac{\int_L [\hat{\tilde{u}}^+ \quad \hat{\tilde{p}}^+]\delta\boldsymbol{H}[\hat{u} \quad \hat{p}]^{\mathrm{T}}\,\mathrm{d}x}{\int_L (\hat{u}\hat{\tilde{u}}^+ + \hat{p}\hat{\tilde{p}}^+)\,\mathrm{d}x}$

TABLE 2. The eigenvalue drift caused by a generic structural perturbation, which is represented by the generic tensor $\delta\boldsymbol{H}$. The two methods, CA_1 and CA_2, are derived from two equivalent versions of the governing equations, § 4. L is the dimensionless tube length.

Method	CA_1	CA_2
$\delta\boldsymbol{H} =$	$\begin{bmatrix} 0 & 0 \\ \delta\beta_c(1-\sigma\tau_c)\delta(x-x_c) & 0 \end{bmatrix}$	$\begin{bmatrix} 0 & 0 \\ \delta\beta_c\delta(x-x_c) & \delta\beta_c\tau_c\delta(x-x_c)\dfrac{\partial}{\partial x} \end{bmatrix}$

TABLE 3. The tensor representing a structural perturbation caused by a second hot wire. Two representations are obtained, depending on whether the heat-release rate is expressed following the CA_1 or CA_2 method.

Method	CA_1	CA_2
$\dfrac{\delta\sigma}{\delta\beta_c} =$	$\dfrac{\hat{\tilde{p}}_c^+\hat{u}_c\,(1-\sigma\tau_c)}{\int_L (\hat{u}\hat{\tilde{u}}^+ + \hat{p}\hat{\tilde{p}}^+)\,\mathrm{d}x + \beta\tau\hat{u}_h\hat{\tilde{p}}_h^+}$	$\dfrac{\hat{\tilde{p}}_c^+\left(\hat{u}_c + \tau_c\dfrac{\partial\hat{p}_c}{\partial x}\right)}{\int_L (\hat{u}\hat{\tilde{u}}^+ + \hat{p}\hat{\tilde{p}}^+)\,\mathrm{d}x}$

TABLE 4. The change in the eigenvalue due to the presence of the control wire with a small heat-release parameter $\delta\beta_c$, derived via the CA_1 and CA_2 approaches.

a manner similar to Giannetti & Luchini (2007). Table 2 describes the effect of a generic perturbation $\delta\boldsymbol{H}$. The great advantage of this approach is that, once the direct and adjoint eigenfunctions have been calculated, all linear feedback mechanisms can be examined at little extra cost.

We will illustrate the process for the specific case where the feedback mechanism is a second hot wire, called the control wire, whose parameters are denoted with the subscript c. The structural perturbation caused by the control wire is represented by the tensor in table 3. The component δH_{21} represents a feedback mechanism that is proportional to the velocity perturbation and that perturbs the pressure equation. The component δH_{22} represents a feedback mechanism that is proportional to the pressure perturbation and that also perturbs the pressure equation. The change in the eigenvalue caused by the presence of the control hot wire with a small heat-release parameter $\delta\beta_c$ is given in table 4 for both CA methods. The results will be described in § 7.2.

6.2. *Base-state sensitivity via the CA method*

Using adjoint techniques, a single calculation can reveal how the growth rate and frequency of the system is altered by any small variation of the base-state

Method	CA_1	CA_2
$\dfrac{\delta\sigma}{\delta\beta} =$	$\dfrac{\hat{\tilde{p}}_h^{+}\hat{u}_h\,(1-\sigma\tau)}{\int_L(\hat{u}\hat{\tilde{u}}^{+}+\hat{p}\hat{\tilde{p}}^{+})\,\mathrm{d}x+\beta\tau\hat{u}_h\hat{\tilde{p}}_h^{+}}$	$\dfrac{\hat{\tilde{p}}_h^{+}\left(\hat{u}_h+\tau\dfrac{\partial\hat{p}_h}{\partial x}\right)}{\int_L(\hat{u}\hat{\tilde{u}}^{+}+\hat{p}\hat{\tilde{p}}^{+})\,\mathrm{d}x}$
$\dfrac{\delta\sigma}{\delta\tau} =$	$\dfrac{-\beta\sigma\hat{\tilde{p}}_h^{+}\hat{u}_h}{\int_L(\hat{u}\hat{\tilde{u}}^{+}+\hat{p}\hat{\tilde{p}}^{+})\,\mathrm{d}x+\beta\tau\hat{u}_h\hat{\tilde{p}}_h^{+}}$	$\dfrac{\beta\hat{\tilde{p}}_h^{+}\dfrac{\partial\hat{p}_h}{\partial x}}{\int_L(\hat{u}\hat{\tilde{u}}^{+}+\hat{p}\hat{\tilde{p}}^{+})\,\mathrm{d}x}$
$\dfrac{\delta\sigma}{\delta\zeta} =$	$\dfrac{-\int_L\hat{p}\hat{\tilde{p}}^{+}\mathrm{d}x}{\int_L(\hat{u}\hat{\tilde{u}}^{+}+\hat{p}\hat{\tilde{p}}^{+})\,\mathrm{d}x+\beta\tau\hat{u}_h\hat{\tilde{p}}_h^{+}}$	$\dfrac{-\int_L\hat{p}\hat{\tilde{p}}^{+}\mathrm{d}x}{\int_L(\hat{u}\hat{\tilde{u}}^{+}+\hat{p}\hat{\tilde{p}}^{+})\,\mathrm{d}x}$

TABLE 5. The change in the eigenvalue due to small changes in the base-state coefficients, derived via the CA_1 and CA_2 methods.

parameters $\delta\beta$, $\delta\zeta$, $\delta\tau$, and δx_h. This is known as the base-state sensitivity. In this section, we calculate the base-state sensitivities to β, τ, and ζ as functions of the hot-wire position, x_h. By applying a methodology similar to that presented in § 6.1, we obtain the base-state sensitivities shown in table 5. The results will be described in § 7.4.

6.3. *Both sensitivities via the DA method*

Both sensitivities can be calculated directly from the discretized governing equations (the DA method). There are four stages to this method: (i) calculate the perturbation matrix $\delta\boldsymbol{P}$ using (A 5), imposing an arbitrarily small perturbation on the base-state parameter; (ii) calculate the eigenvectors of the matrices $\boldsymbol{\Gamma}$ and $-\boldsymbol{\Gamma}^H$; (iii) apply (6.2) below to find the eigenvalue drift; (iv) divide the eigenvalue drift by the perturbation used in stage 1 in order to obtain the sensitivity coefficient. The eigenvalue drift due to a perturbation of the discretized direct system (similar to Giannetti & Luchini 2007) is given by

$$\delta\sigma = \frac{\hat{\tilde{\boldsymbol{\xi}}}\cdot\left(\delta\boldsymbol{P}\hat{\boldsymbol{\chi}}\right)}{\hat{\tilde{\boldsymbol{\xi}}}\cdot\hat{\boldsymbol{\chi}}}, \tag{6.2}$$

where the matrix $\delta\boldsymbol{P}$ represents a small perturbation to the direct system, whose matrix is $\boldsymbol{\Gamma}$. Here, the symbol $\hat{}$ represents an eigenvector. The column vector $\hat{\boldsymbol{\xi}}$ is the eigenvector of the adjoint matrix $\boldsymbol{\Phi} = -\boldsymbol{\Gamma}^H$. The perturbation matrix $\delta\boldsymbol{P}$ is given in (A 5). It can represent either a structural perturbation or a base-state perturbation.

7. Results and physical interpretation

7.1. *Comparing the three methods of calculating the structural sensitivity*

Figure 5(*a,b*) shows the real and imaginary components of $\delta\sigma/\delta\beta_c$ as a function of the control wire position, x_c, via the DA, CA_1 and CA_2 methods. In this case the main hot wire is placed at $x = 0.25$ so that most of the perturbation energy is in the first acoustic mode (Matveev 2003). Figure 6(*a,b*) is the same as figure 5(*a,b*) but the main

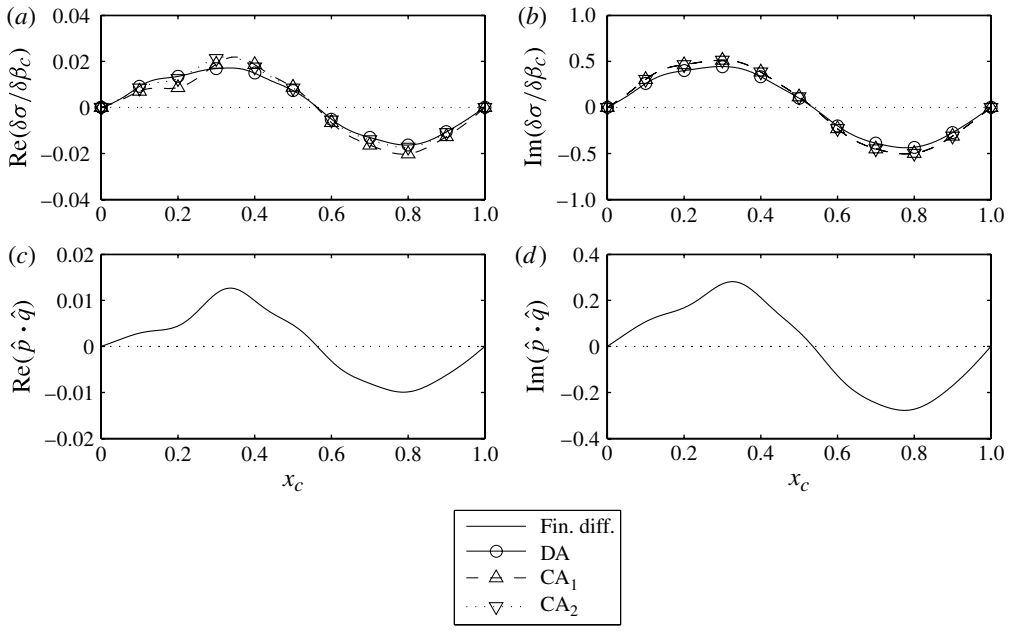

FIGURE 5. (*a,b*) Sensitivity of the growth rate, $\mathrm{Re}(\delta\sigma/\delta\beta_c)$, and of the angular frequency, $\mathrm{Im}(\delta\sigma/\delta\beta_c)$, when a control wire is placed at position x_c. This is calculated exactly, via finite difference, and via the DA, CA_1 and CA_2 methods. (The DA method gives the same result as the finite-difference method to machine precision.) (*c,d*) The Rayleigh index for a control wire placed at x_c. The parameters are $N = 10$, $\beta = 0.5$, $c_1 = 0.01$, $c_2 = 0.004$ and $\tau = \tau_c = 0.01$. The main hot wire is at $x_h = 0.25$ so that the first acoustic mode is excited.

hot wire is now placed at $x = 0.625$ so that most of the perturbation energy is in the second acoustic mode (Matveev 2003). These results can be compared with the exact solution, which is obtained by finite difference. This is the difference between the dominant eigenvalues of the perturbed direct matrix, $\boldsymbol{\Gamma} + \delta\boldsymbol{P}$, and the original direct matrix, $\boldsymbol{\Gamma}$, divided by the (finite) arbitrarily small perturbation. The perturbation matrix $\delta\boldsymbol{P}$ is given in (A 5).

As expected, the DA method matches the finite difference method exactly. The CA methods both contain some error, due to the truncation errors in the discretization. The CA_2 method is usually more accurate than the CA_1 method. For this thermo-acoustic system, however, the DA method turns out to be the most accurate and easy to implement.

The real component of the structural sensitivity gives the change in the growth rate that is caused by the control wire. The imaginary component gives the change in the frequency. The physical reason for these changes is given in § 7.2. The control wire has a much stronger effect on the frequency than on the growth rate, for reasons given in § 7.3.

7.2. *Comparing the structural sensitivity with the Rayleigh Index*

It has long been known (Rayleigh 1878) that if pressure and heat-release fluctuations are in phase, then acoustic vibrations are encouraged. More precisely, the Rayleigh Criterion states that the energy of the acoustic field grows over one cycle of oscillation if $\oint_T \int_{\mathscr{D}} p\dot{q}\,\mathrm{d}\mathscr{D}\,\mathrm{d}t$ exceeds the damping, where $\mathscr{D}$ is the flow domain and T is the

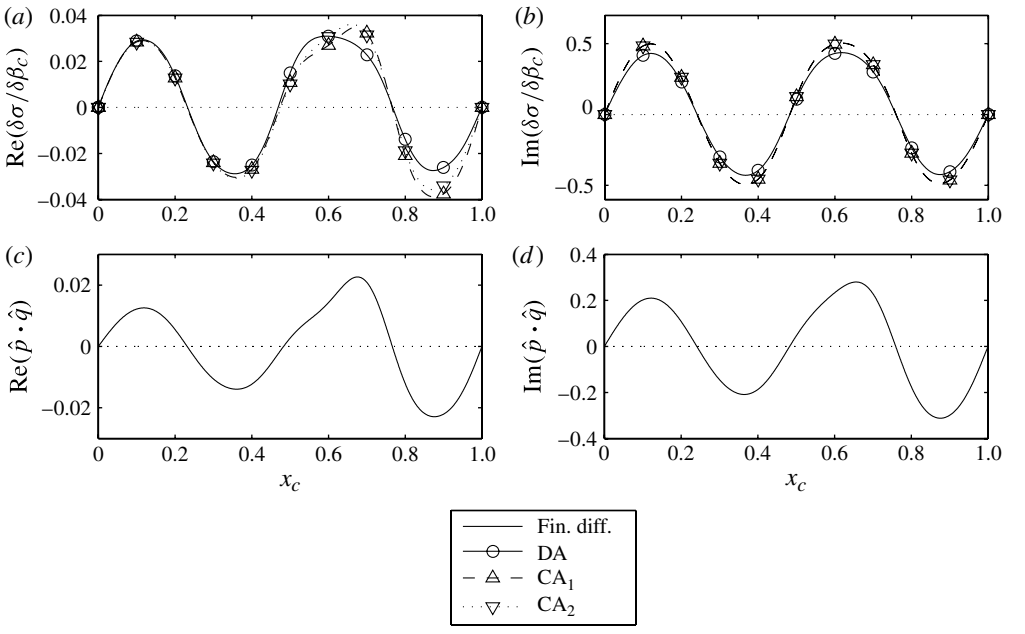

FIGURE 6. (*a,b*) Sensitivity of the growth rate, $\mathrm{Re}(\delta\sigma/\delta\beta_c)$, and of the angular frequency, $\mathrm{Im}(\delta\sigma/\delta\beta_c)$, when a control wire is placed at position x_c. This is calculated exactly, via finite difference, and via the DA, CA_1 and CA_2 methods. (The DA method gives the same result as the finite-difference method to machine precision.) (*c,d*) The Rayleigh index for a control wire placed at x_c. The parameters are $N = 10$, $\beta = 0.5$, $c_1 = 0.01$, $c_2 = 0.004$ and $\tau = \tau_c = 0.01$. The main hot wire is at $x_h = 0.625$ so that the second acoustic mode is excited.

period. It is particularly informative to plot the spatial distribution of

$$\oint_T p\dot{q}\,\mathrm{d}t \tag{7.1}$$

which is known as the Rayleigh Index. This reveals the regions of the flow that contribute most to the Rayleigh Criterion and therefore gives insight into the physical mechanisms that alter the amplitude of the oscillation. To examine the effect of the control wire, we substitute the approximate expressions $p = \hat{p}\exp(\sigma_i t)$ and $\dot{q} = \hat{\dot{q}}\exp(\sigma_i t)$ (found from (2.4) or (2.5)) into (7.1) and integrate over a period $2\pi/\sigma_i$, where $\sigma_i = \mathrm{Im}(\sigma)$. (The approximation arises because the growth rate over the cycle has been ignored.) The real part of the Rayleigh Index gives the change in the growth rate and the imaginary part gives the change in the frequency (figures 5*c,d*), 6*c,d*). As expected, the sign of the Rayleigh index matches that of the structural sensitivity (the position at which it is zero matches within 1 %) and the shape is similar. The Rayleigh Index physically explains the effect of adding the control hot wire to the Rijke tube.

First, we refer to figure 5 where the main hot wire is at $x_h = 0.25$ and most of the perturbation energy is contained in the first mode. For $x = 0$–0.56, the pressure and heat-release eigenfunctions are sufficiently in phase that the contribution to growth over a cycle is positive. For $x = 0.56$–1, they are out of phase so their contribution to growth over a cycle is negative. For this case, the location where the presence of a second hot wire is most effective at reducing the growth rate is $x_c \approx 0.8$. It is interesting to note that this system becomes more unstable when the control wire is

Method	CA_1	CA_2
$\boldsymbol{S} = \dfrac{\delta\sigma}{\delta \boldsymbol{C}} =$	$\dfrac{[\hat{\tilde{u}}^+ \quad \hat{\tilde{p}}^+]^{\mathrm{T}} \otimes [\hat{u} \quad \hat{p}]^{\mathrm{T}}}{\int_L (\hat{u}\hat{\tilde{u}}^+ + \hat{p}\hat{\tilde{p}}^+)\,\mathrm{d}x + \beta\tau \hat{u}_h \hat{\tilde{p}}_h^+}$	$\dfrac{[\hat{\tilde{u}}^+ \quad \hat{\tilde{p}}^+]^{\mathrm{T}} \otimes [\hat{u} \quad \hat{p}]^{\mathrm{T}}}{\int_L (\hat{u}\hat{\tilde{u}}^+ + \hat{p}\hat{\tilde{p}}^+)\,\mathrm{d}x}$

TABLE 6. Structural sensitivity tensor for a general feedback mechanism $\delta\boldsymbol{C}$.

placed at $0.5 < x_c < 0.56$. This is in the second half of the tube and, in the absence of the first hot wire, a control wire placed here would be stabilizing. The reason for this is that the main hot wire, at x_h, causes the eigenfunctions to distort from the acoustic modes of the duct. In particular, the features of the $\hat{u}$ and $\hat{p}$ eigenfunctions (figure 2) shift down the duct, to higher values of x. This shifts downstream the region in which the control wire is destabilizing.

Secondly, we refer to figure 6 where the main hot wire is at $x_h = 0.625$ and most of the perturbation energy is contained in the second mode. For $0 < x < 0.23$ and $0.47 < x < 0.77$, the pressure and heat-release eigenfunctions are sufficiently in phase that the contribution to growth over a cycle is positive; for $0.23 < x < 0.47$ and $0.77 < x < 1$, they are out of phase so their contribution to growth over a cycle is negative. For this case, the location where the presence of a second hot wire is most effective at reducing the growth rate is $x_c \approx 0.36$.

7.3. *Using the structural sensitivity to find the most efficient feedback mechanisms*

In passive control, an object that is placed at a point in the system causes feedback at that point. Under these conditions, the structural sensitivity reveals the feedback mechanism that is most effective at changing the frequency or growth rate of the system.

In § 6.1, we defined the perturbation tensor, $\delta\boldsymbol{H}$, to be an operator localized at the control wire's location. In this section we consider the case of a generic feedback mechanism, represented by a localized perturbation in which $\delta\boldsymbol{H}$ is constant, following Giannetti & Luchini (2007). For clarity, we re-label $\delta\boldsymbol{H}$ as $\delta\boldsymbol{C}$ for this case. The *structural sensitivity tensor* $\boldsymbol{S} = \delta\sigma/\delta\boldsymbol{C}$ is then given by the expression in table 6. Its numerator is the dyadic product $[\hat{\tilde{u}}^+ \quad \hat{\tilde{p}}^+]^{\mathrm{T}} \otimes [\hat{u} \quad \hat{p}]^{\mathrm{T}}$. The four components of $\boldsymbol{S}$ quantify how a feedback mechanism that is proportional to the state variables affects the growth rate and frequency of the system. They are shown in figure 7 (real part) and figure 8 (imaginary part) as a function of x, which is the location of the structural perturbation. The eigenfunctions are calculated with both 10 modes (thick line) and 100 modes (thin line). With the latter discretization it is possible to capture the eigenfunction discontinuity at the hot-wire location caused by the impulsive heat release. Although a discretization with 100 modes does not meet the physical constraint that $\tau \ll 2/N$ (§ 3), we can use it to examine the numerical accuracy of the 10-mode discretization. At the hot-wire location, the 100-mode discretization of $\mathrm{Re}(S_{12})$ and $\mathrm{Im}(S_{11})$ experiences the Gibbs phenomenon (Gibbs 1898) and therefore the solution is inaccurate. The Gibbs phenomenon remains as the number of Galerkin modes increases. The 10-mode discretization is very accurate except at the discontinuity at the hot-wire location.

When $\beta \to 0$, the direct eigenfunctions are nearly the acoustic modes of the system, as shown in figures 2 and 3. By inspection of these eigenfunctions, we

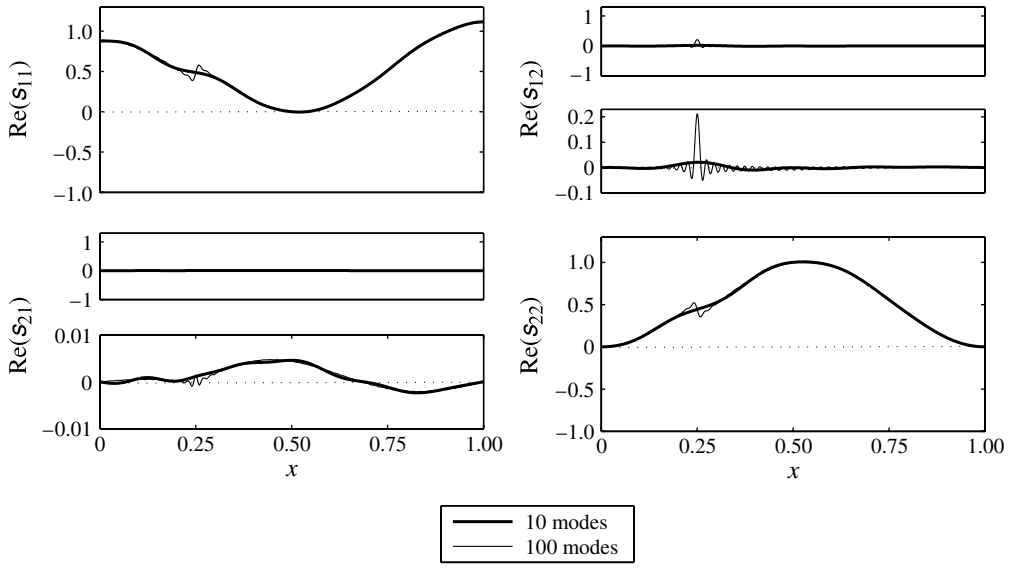

FIGURE 7. Real part of the components of the structural sensitivity tensor (via the DA method) for the same parameters as figure 5. These components indicate the effect of a feedback mechanism on the growth rate of oscillation.

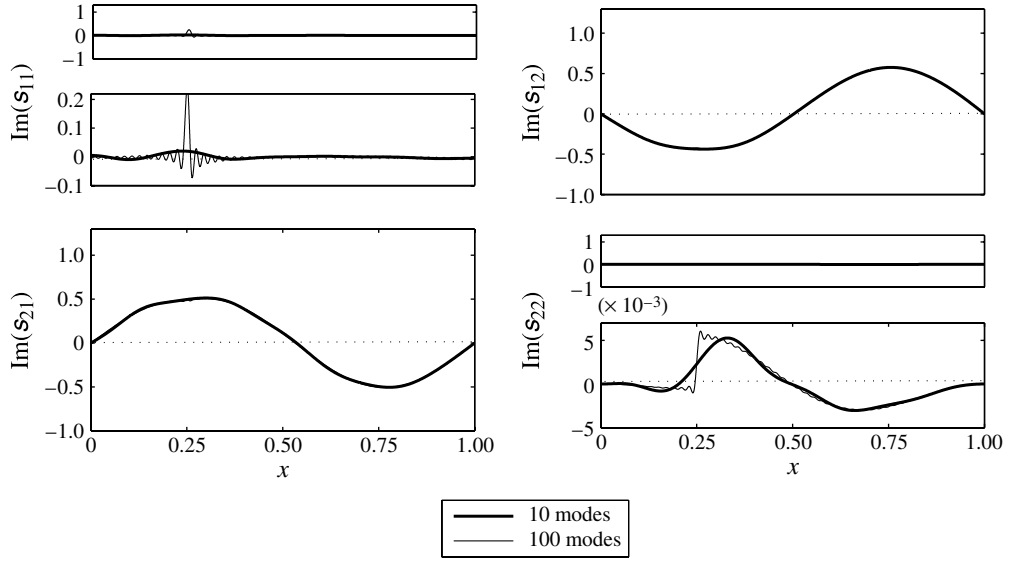

FIGURE 8. Imaginary part of the components of the structural sensitivity tensor (via the DA method) for the same parameters as figure 5. These components indicate the effect of a feedback mechanism on the angular frequency of oscillation.

see that $S_{11} \approx (\cos \pi x)^2$, $S_{12} \approx -\mathrm{i}(\sin \pi x) \times (\cos \pi x)$, $S_{21} \approx \mathrm{i}(\sin \pi x) \times (\cos \pi x)$ and $S_{22} \approx (\sin \pi x)^2$, when $\beta \to 0$. The heat release from the main hot wire distorts these eigenfunctions (figure 2) so the structural sensitivities are similarly distorted.

First, we consider a feedback mechanism that is proportional to the velocity and that forces the momentum equation (S_{11}). For example, this could be caused by the drag from a fine mesh placed in the flow. The system is most sensitive when this feedback mechanism is placed at the entrance or exit of the duct. This is because: (i) the velocity mode is maximal there; and (ii) the adjoint velocity, which is a measure of the sensitivity of the momentum equation, is also maximal there, as shown in figure 4. The $\mathrm{Re}(S_{11})$ component (figure 7) is positive for all values of x, which means that, whatever value of x is chosen, the growth rate will decrease if the forcing is in the opposite direction to the velocity, as it would be for a fine mesh placed in the flow. This type of feedback greatly affects the growth rate (figure 7), which is the real component of the sensitivity, but barely affects the frequency (figure 8), which is the imaginary component. This behaviour is as expected for this type of feedback.

Secondly, we consider a feedback mechanism that is proportional to the pressure and that forces the pressure equation (S_{22}). This type of feedback is described in Chu (1963) and is relevant to pressure-coupled heat release in solid rocket engines. For this feedback, the system is most sensitive around the centre of the duct, with a maximum at $x \approx 0.58$. Again, this feedback greatly affects the growth rate (figure 7), and it is positive for all values of x, but barely affects the frequency (figure 8). If the heat release increases with the pressure, as it does for most chemical reactions, this feedback mechanism is destabilizing.

Thirdly, we consider S_{12}, which represents feedback from the pressure into the momentum equation, and S_{21}, which represents feedback from the velocity into the pressure equation. These types of feedback barely affect the growth rate (figure 7) but greatly affect the frequency (figure 8). The hot control wire considered in figure 5 causes this type of feedback (S_{21}) if $\tau = 0$. This analysis shows, therefore, that this passive control device is quite ineffective at reducing the growth rate. This had been shown already in figure 5, in which the hot wire is seen to affect the frequency (imaginary component) much more than it affects the growth rate (real component).

By inspection of figure 7, we conclude that the passive device that is most effective at reducing the growth rate should force the momentum equation in the opposite direction to the velocity fluctuation and should be placed at the exit of the tube. A damping device such as an adiabatic wire mesh would achieve this.

This paper is mainly relevant to passive control but it is worth briefly mentioning active control. For active control, the sensor and actuator would typically be in different places. For maximum observability, the sensor should be placed where the relevant direct eigenfunction has its largest amplitude. For maximum controllability, the actuator should be placed where the relevant adjoint eigenfunction has its largest amplitude.

7.4. *Base-state sensitivity results*

Figure 9(*a*) shows how a small variation in the heat-release parameter, β, affects the growth rate, $\mathrm{Re}(\sigma)$, and the angular frequency, $\omega \equiv \mathrm{Im}(\sigma)$, for different hot-wire positions, x_h. Figure 9(*b*) shows how a small variation in the time-delay coefficient, τ, affects the same quantities. These are calculated via the DA, CA_1, and CA_2 methods and the results are checked against the exact solution, which is obtained by finite difference, as in § 6.1.

As shown in table 5, these curves depend on the shapes of the direct and adjoint eigenfunctions. In turn, these eigenfunctions are distorted from the natural acoustic modes of the duct by the heat release from the wire. (This distortion is shown in figures 2 and 3 for $x_h = 0.25$.) This accounts for the elaborate shapes of the base-state

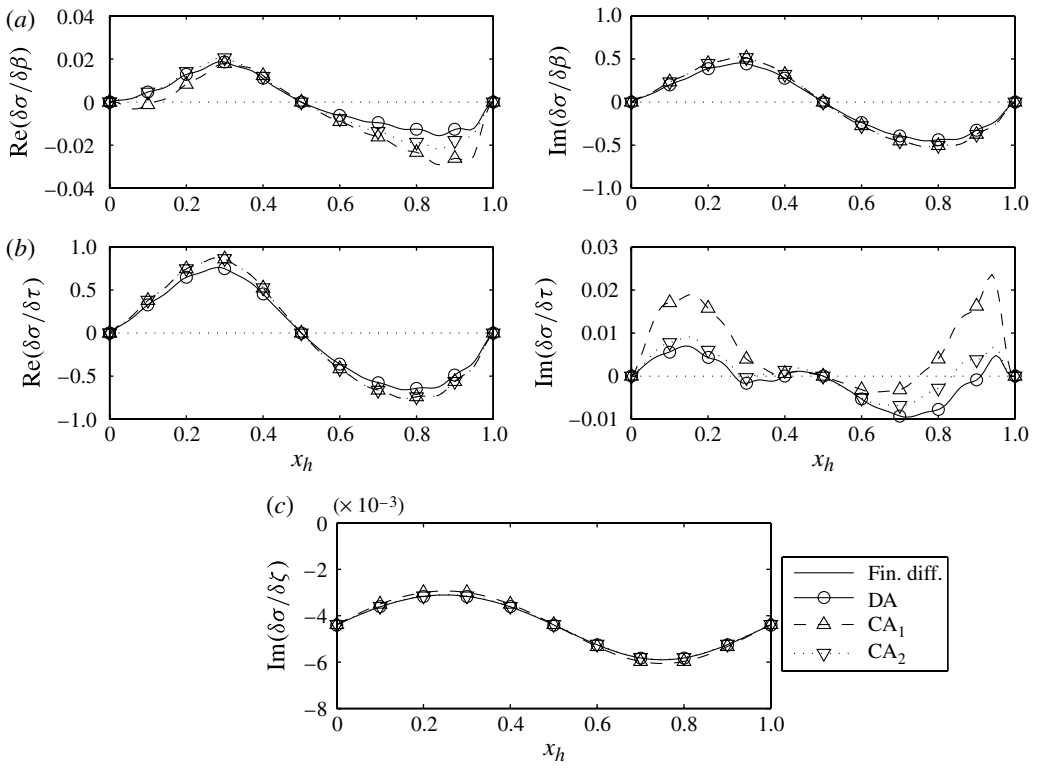

FIGURE 9. Sensitivity to base-state modifications of β (a), τ (b) and ζ (c). The mean values are $\tau = 0.01$, $\beta = 0.5$, $c_1 = 0.05$ and $c_2 = 0.005$. For the analysis of β and τ 10 Galerkin modes are considered, whereas for ζ only the first mode is considered.

sensitivity curves. It is also worth commenting on their relative magnitudes: small variations in β have a much greater effect on the frequency than on the growth rate, while small variations in τ have a much greater effect on the growth rate than on the frequency. This will always be the case when $\omega\tau \ll 1$, which is easy to justify by the following argument. If $p \sim \sin\omega t$ at the hot wire, then $u \sim \cos\omega t$ and $\dot{q} \sim \cos\omega(t-\tau)$ there. Using trigonometric relations, it is easy to show that $\oint p\dot{q}\,\mathrm{d}t$, which quantifies how much β affects the growth rate, is proportional to $\sin\omega\tau$ and that $\oint u\dot{q}\,\mathrm{d}t$, which quantifies how much β affects the frequency, is proportional to $\cos\omega\tau$. Therefore, for small $\omega\tau$, the change in the growth rate, $\mathrm{Re}(\delta\sigma/\delta\beta)$, should be of order $\omega\tau$, while the change in the frequency, $\mathrm{Im}(\delta\sigma/\delta\beta)$, should be of order 1. Differentiating with respect to τ at constant β, we find that the change in $\oint p\dot{q}\,\mathrm{d}t$ due to a change in τ is proportional to $\omega\cos\omega\tau$. Similarly, the change in $\oint u\dot{q}\,\mathrm{d}t$ due to a change in τ is proportional to $\omega\sin\omega\tau$. Therefore, for small $\omega\tau$, $\mathrm{Re}(\delta\sigma/\delta\tau)$ should be of order ω, while $\mathrm{Im}(\delta\sigma/\delta\beta)$ should be of order $\omega^2\tau$. These magnitudes closely match the amplitudes in figure 9, for which $\omega \approx \pi$ and $\tau = 0.01$.

Figure 9(c) shows how the angular frequency changes with the damping factor ζ. A small increase in ζ lowers the frequency of the linear oscillations. A small increase of ζ is always stabilizing, i.e. the growth rate decreases, but does not depend on the hot-wire position (figure not shown). In order to study the sensitivity to small changes

of the damping, $\delta\zeta$, only one Galerkin mode has been considered. This is because ζ is a function of the Galerkin mode, as explained in § 3. Therefore, with the damping model and numerical discretization adopted, formulae in the bottom row of table 5 are valid only for the first Galerkin mode.

As for the structural sensitivity, there is a discrepancy between the DA and CA solutions, which arises from the different truncation errors in the discretizations. The origin of this error can be inferred from the matrices in appendix A. The CA_1 method provides an inaccurate $\mathrm{Im}(\delta\sigma/\delta\tau)$, as shown in figure 9(*b*). This is due to the time-delay coefficient and this discrepancy vanishes as the time delay becomes much smaller. In this case, we find that the maximal discrepancy between CA_1 and the exact solution is smaller than 10 % when $\tau < 0.001$.

8. Passive control of an unstable system

In this section we demonstrate the suppression of thermo-acoustic oscillations using a control wire placed at the optimal location, as predicted by the structural sensitivity analysis. We use the parameters in figure 5, which shows that, in order to reduce the growth rate most effectively, the control wire should be placed at $x_c = 0.8$. We integrate the nonlinear time-delayed governing equations given in appendix B, (B 1)–(B 2), forward in time with a fourth-order Runge–Kutta algorithm and 20 Galerkin modes.

When the control wire is absent, the growth rate is $\sigma_r = 0.00023$ and the angular frequency is $\sigma_i = 3.3570$. We set the heat-release parameter for the control wire to be $\beta_c = \beta/10 = 0.05$, which is small enough to fulfil the linear assumptions. When the control wire is present, the growth rate is $\sigma_r = -0.00058$ and the angular frequency is $\sigma_i = 3.3354$. The difference between these values matches that predicted by the structural sensitivity analysis, for which $\delta\sigma = \beta_c \times \delta\sigma/\delta\beta_c \approx 0.05 \times (-0.01633 - 0.4323\mathrm{i}) = -0.00082 - 0.02162\mathrm{i}$, at $x_c = 0.8$.

Figure 10(*a*) shows the pressure at $x = 0.25$ as a function of time in the nonlinear simulations. The control wire is introduced at $t = 1000$. The behaviour is as expected: there is exponential growth until $t = 1000$ and exponential decay afterwards. In figure 10(*b–c*) the fast Fourier transform (FFT) performed on the nonlinear time-solution confirms the frequency shift predicted by the sensitivity analysis.

9. Conclusions

The main goal of this paper is to take a technique developed for the analysis of hydrodynamic stability and adapt it to the analysis of thermo-acoustic stability. This technique uses adjoint equations to calculate a system's sensitivity to feedback or to changes in the base state.

By arranging the linearized thermo-acoustic governing equations in two different ways, we derive two different sets of adjoint equations, which we then discretize with a Galerkin decomposition. This is known as the 'continuous adjoint' (CA) method and the two sets of adjoint equations produce two different matrices, labelled CA_1 and CA_2. We also derive the adjoint equations directly from the discretized linearized thermo-acoustic system. This is known as the 'discrete adjoint' (DA) method and it produces another matrix, labelled DA. The DA matrix is the negative Hermitian of the matrix representing the discretized governing equations. We calculate the direct and adjoint eigenfunctions of the thermo-acoustic system using these direct and adjoint matrices. We find that the DA method is more accurate and easier to implement than either CA method for this thermo-acoustic model.

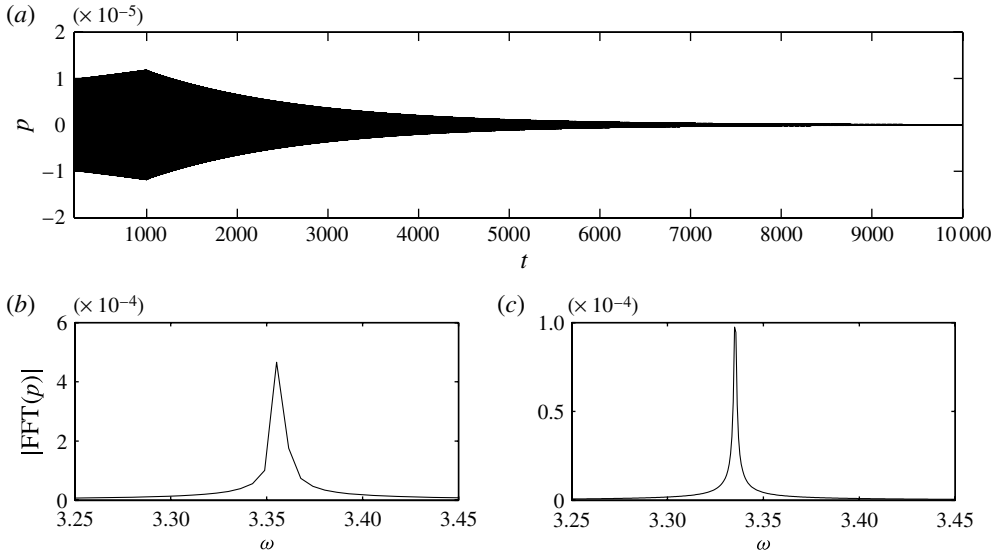

FIGURE 10. Stabilization of the thermo-acoustic system via a second hot wire introduced at $t = 1000$ and $x_c = 0.8$. $\beta_c = \beta/10 = 0.05$ and the remaining parameters are the same as in figure 5. The time integration (*a*) is performed on the nonlinear time-delayed equations discretized with 20 Galerkin modes. The solution is shown at $x = 0.25$. The amplitude of the spectrum of the solution is shown in (*b*) for $t < 1000$ and (*c*) for $t > 1000$.

Two sensitivity analyses are carried out: one focuses on structural perturbations and the other on base-state perturbations. In the structural sensitivity analysis, we calculate the effect that a generic feedback mechanism has on the frequency and growth rate of oscillations. We illustrate this by considering the influence of a second hot wire, with a small heat-release parameter. We find that the second wire affects the frequency much more than the growth rate and explain this physically by evaluating the Rayleigh Index for the second hot wire. We then use the results of the structural sensitivity to identify the feedback mechanism that is most effective at reducing the growth rate of oscillations. We find that this mechanism should force the momentum equation in the opposite direction to the velocity perturbation and that it should be placed at the downstream end of the duct. An adiabatic fine mesh would achieve this. In the base-state sensitivity analysis, we calculate the effect that a small variation in the base-flow parameters has on the frequency and growth rate of oscillations. As expected, we find that a small increase in the wire temperature affects the frequency more than the growth rate and that a small increase in the time delay affects the growth rate more than the frequency. Also as expected, we find that a small increase in the damping always has a stabilizing effect. The novelty of this paper is in the technique. Each sensitivity analysis was obtained extremely quickly with a single calculation. It was then checked against the exact solution found by many finite-difference calculations. The DA method matched the finite-difference method exactly, while there was some discrepancy when using the CA_1 and CA_2 methods.

The successful application of sensitivity analysis to thermo-acoustics opens up new possibilities for the passive control of thermo-acoustic oscillations. In a single calculation, sensitivity analysis shows how the growth rate and frequency of small oscillations about some base state are affected either by a passive control element in

the system or by a change to its base state. This gradient information can be combined with other constraints, such as that the total mean heat release be constant, to show how an unstable thermo-acoustic system should be changed in order to make it stable. In this paper, we have demonstrated this for a simple system with four elements to the base state: the hot-wire position, its heat-release coefficient, its time delay and the damping. In future work, we will examine more elaborate flame models and acoustic networks. This will allow us to calculate the sensitivity to the flame shape and to the characteristics of the acoustic network in which the flame sits.

Acknowledgements

We would like to thank Dr O. Tammisola (Department of Engineering, University of Cambridge, UK) for valuable discussions and comments on this paper. This work was supported by the European Research Council through Project ALORS 2590620.

Appendix A. Discretized equations

It is useful to define the following matrices, which are expressed in matrix notation (repeated indices are not to be summed):

$$\left.\begin{aligned} &A_{ij} \equiv 0, \quad B_{ij} \equiv \pi\delta_{ij} i, \quad E_{ij}(c_1, c_2) \equiv -\zeta_i \delta_{ij}, \\ &F_{ij}(\beta_w, x_w) \equiv -2\beta_w \sin(\pi i x_w)\cos(\pi j x_w), \\ &G_{ij}(\beta_w, x_w, \tau_w) \equiv 2i\pi\tau_w\beta_w \sin(\pi i x_w)\cos(\pi j x_w), \\ &H_{ij}(\beta_w, x_w, \tau_w, c_1, c_2) \equiv 2\beta_w\tau_w\zeta_j \cos(\pi i x_w)\sin(\pi j x_w), \\ &C_{ij}(\beta_w, x_w) \equiv -B_{ij} + F_{ij}, \quad D_{ij}(\beta_w, x_w, \tau_w, c_1, c_2) \equiv E_{ij} + G_{ij}, \end{aligned}\right\} \tag{A 1}$$

where $i, j = 1, 2, \ldots, N$, N is the number of Galerkin modes, δ_{ij} is the Kronecker delta and w stands for wire. The direct matrix $\boldsymbol{\Gamma}$ is given by:

$$\boldsymbol{\Gamma} = \begin{bmatrix} \boldsymbol{A} & \boldsymbol{B} \\ \boldsymbol{C}(\beta_h, x_h) & \boldsymbol{D}(\beta_h, x_h, \tau_h, c_1, c_2) \end{bmatrix}. \tag{A 2}$$

The CA equations (table 1) are discretized using the Galerkin method as for the direct modes, by means of the decomposition in (3.1). The discretization of the first set of adjoint equation CA_1 (table 1) gives rise to the following adjoint matrix:

$$\boldsymbol{\Phi} = \begin{bmatrix} -\boldsymbol{G}^{\mathrm{T}}(\beta_h, x_h, \tau_h) & \boldsymbol{B} - \boldsymbol{F}^{\mathrm{T}}(\beta_h, x_h) + \boldsymbol{H}(\beta_h, x_h, \tau_h, c_1, c_2) \\ -\boldsymbol{B} & -\boldsymbol{E}(c_1, c_2) \end{bmatrix}, \tag{A 3}$$

while the second set CA_2 (table 1) gives the following adjoint matrix:

$$\boldsymbol{\Phi} = \begin{bmatrix} \boldsymbol{A} & \boldsymbol{B} - \boldsymbol{F}^{\mathrm{T}}(\beta_h, x_h) \\ -\boldsymbol{B} & -\boldsymbol{E}(c_1, c_2) + \boldsymbol{G}^{\mathrm{T}}(\beta_h, x_h, \tau_h) \end{bmatrix}. \tag{A 4}$$

Note that $\boldsymbol{\Gamma}$ and $\boldsymbol{\Phi}$ are $2N \times 2N$ matrices. We indicated the main hot wire with subscript h and the control hot wire with the subscript c. Finally, the perturbation

matrix of the direct system is:

$$\delta \boldsymbol{P} = \begin{bmatrix} [0]_{N\times N} & [0]_{N\times N} \\ \boldsymbol{C}(\beta_h + \delta\beta_h, x_h) + \cdots & \boldsymbol{D}(\beta_h + \delta\beta_h, x_h, \tau_h + \delta\tau_h, c_1 + \delta c_1, c_2 + \delta c_2) + \cdots \\ \cdots + \boldsymbol{C}(\delta\beta_c, x_c) & \cdots + \boldsymbol{D}(\delta\beta_c, x_c, \delta\tau_c, c_1, c_2) \end{bmatrix}. \tag{A 5}$$

On the one hand, we obtain the perturbation matrix caused by the presence of the second hot wire by setting $\delta\beta_h = \delta\tau_h = \delta c_1 = \delta c_2 = 0$ and $\delta\beta_c > 0$ and $\delta\tau_c > 0$. On the other hand, we obtain the perturbation matrix caused by (positive) base-state variations by setting $\delta\beta_c = \delta\tau_c = 0$ and $\delta\beta_h > 0$, $\delta\tau_h > 0$, $\delta c_1 > 0$ and $\delta c_2 > 0$.

Appendix B. Nonlinear time-delayed equations for control

In this section we provide the nonlinear time-delayed equations of the thermo-acoustic system with a control hot wire.

Referring to the time integration presented in § 8, when the second hot wire is off, for $t < 1000$, then $\beta_c = 0$; when the second wire is on, for $t \geqslant 1000$, then $\beta_c = \beta/10$.

$$\frac{\partial u}{\partial t} + \frac{\partial p}{\partial x} = 0, \tag{B 1}$$

$$\frac{\partial p}{\partial t} + \frac{\partial u}{\partial x} + \zeta p - \frac{2}{\sqrt{3}}\beta \left(\left| \frac{1}{3} + u(t-\tau) \right|^{1/2} - \left(\frac{1}{3} \right)^{1/2} \right) \delta(x - x_h) + \cdots$$

$$\cdots - \frac{2}{\sqrt{3}}\beta_c \left(\left| \frac{1}{3} + u(t-\tau_c) \right|^{1/2} - \left(\frac{1}{3} \right)^{1/2} \right) \delta(x - x_c) = 0. \tag{B 2}$$

REFERENCES

BALASUBRAMANIAN, K. & SUJITH, R. I. 2008*a* Thermoacoustic instability in a Rijke tube: non-normality and nonlinearity. *Phys. Fluids* **20**, 044103.

BALASUBRAMANIAN, K. & SUJITH, R. I. 2008*b* Non-normality and nonlinearity in combustion-acoustic interaction in diffusion flames. *J. Fluid Mech.* **594**, 29–57.

BELEGUNDU, A. D. & ARORA, J. S. 1985 A sensitivity interpretation of adjoint variables in optimal design. *Comput. Meth. Appl. Mech. Engng* **48**, 81–89.

CHANDLER, G. J., JUNIPER, M. P., NICHOLS, J. W. & SCHMID, P. J. 2012 Adjoint algorithms for the Navier–Stokes equations in the low Mach number limit. *J. Comput. Phys.* **231**, 1900–1916.

CHU, B. T. 1963 Analysis of a self-sustained thermally driven nonlinear vibration. *Phys. Fluids* **6** (11), 1638–1644.

CULICK, F. E. C. 1971 Nonlinear growth and limiting amplitude of acoustic oscillations in combution chambers. *Combust. Sci. Technol.* **3**, 1–16.

DENNERY, P. & KRZYWICKI, A. 1996 *Mathematics for Physicists*. Dover.

GIANNETTI, F., CAMARRI, S. & LUCHINI, P. 2010 Structural sensitivity of the secondary instability in the wake of a circular cylinder. *J. Fluid Mech.* **651**, 319–337.

GIANNETTI, F. & LUCHINI, P. 2007 Structural sensitivity of the first instability of the cylinder wake. *J. Fluid Mech.* **581**, 167–197.

GIBBS, J. W. 1898 Fourier's series. *Lett. Nature* **59**, 200.

HECKL, M. 1990 Nonlinear acoustic effects in the Rijke tube. *Acustica* **72**, 63.

HILL, D. C. 1992 A theoretical approach for analysing the restabilization of wakes, *NASA TM* 103858.

JUNIPER, M. P. 2011 Triggering in the horizontal Rijke tube: non-normality, transient growth and bypass transition. *J. Fluid Mech.* **667**, 272–308.

LANDAU, L. D. & LIFSHITZ, E. M. 1959 *Fluid Mechanics*. Pergamon.

MARQUET, O., SIPP, D. & JACQUIN, L. 2008 Sensitivity analysis and passive control of cylinder flow. *J. Fluid Mech.* **615**, 221–252.

MATVEEV, I. 2003 Thermo-acoustic instabilities in the Rijke tube: experiments and modelling. PhD thesis, CalTech.

RAYLEIGH, LORD 1878 The explanation of certain acoustical phenomena. *Nature* **18**, 319–321.

SALWEN, H. & GROSCH, C. E. 1981 The continuous spectrum of the Orr–Sommerfeld equation. Part 2. Eigenfuction expansions. *J. Fluid Mech.* **104**, 445–465.

SIPP, D., MARQUET, O., MELIGA, P. & BARBAGALLO, A. 2010 Dynamics and control of global instabilities in open-flows: a linearized approach. *Appl. Mech. Rev.* **63** (3), 030801.